Sedimentary Geology 235 (2011) 188–199

Contents lists available at ScienceDirect

Sedimentary Geology

journal homepage: www.elsevier.com/locate/sedgeo

Holocene soft-sediment deformation of the Santa Fe–Sopetrán Basin, northern Colombian Andes: Evidence for pre-Hispanic seismic activity?

F. Suter [a,*], J.I. Martínez [a,1], M.I. Vélez [b,2]

[a] Departamento de Geología, Área de Ciencias del Mar, Universidad EAFIT, Medellín, Colombia
[b] Geology Department, University of Regina, Canada

ARTICLE INFO

Article history:
Received 29 January 2010
Received in revised form 18 July 2010
Accepted 24 September 2010
Available online 29 September 2010

Keywords:
Triggering mechanism
Driving force
Seismite
Paleoseismology
Geologic risk
Cauca–Romeral Fault System

ABSTRACT

The detailed study of four deformed intervals from the Holocene fluvio-lacustrine deposits of the Santa Fe–Sopetrán Basin in northern Colombia shows 17 types of soft-sediment deformation (SSD) structures. Evidence indicates that seismic activity was responsible for the SSD structures, a conclusion reached after considering the environmental conditions at the time of sediment deposition and shortly after, and the detailed analysis of the driving force systems. Other triggers (i.e. overloading and rapid sedimentation), however, are not discarded. Intervals showing SSD structures occurred at centennial frequencies and apparently resulted from Mw 6–7 earthquakes. The Holocene age of these major shaking events should be seriously considered when evaluating the seismic hazard and risk for the middle Cauca Valley and the nearby city of Medellín with 3 million inhabitants.

1. Introduction

Soft-sediment deformation (SSD) occurs during or just after deposition, when sediment is still unconsolidated (Maltman, 1994). It results from the combination of a deformation mechanism, which allows sediment to behave temporarily as a fluid (i.e. liquidization, Allen, 1977), and a driving force, which is latent in the sediment under normal conditions and manifests later on when liquidization occurs (Owen, 1987, 1996, 2003). The most common liquidization processes are liquefaction, fluidization, or thixotropy (Owen, 2003). Possible driving forces include, among others, inverse density gradient, uneven loading, horizontal shear stress, and vertical shear (Owen, 1987, 1996). In order for soft sediments to deform, the deformation mechanism must be triggered. Triggering agents can be linked to depositional processes or be external and independent. They include: (1) cyclical pressure fluctuations associated with waves and storm waves (e.g. Eyles and Clark, 1986; Molina et al., 1998; Alfaro et al., 2002) or turbulent flow, (2) impulsive stress or impacts associated with waves (e.g. Dalrymple, 1979, 1980) or flow fronts, (3) tides (e.g. Greb and Archer, 2007), (4) artesian water rise due to base-level fluctuations (e.g. Massari et al., 2001) or floods (e.g. Li et al., 1996), (5) overriding ice dynamics (e.g. Lee and Phillips, 2008; Denis et al., 2009), or (6) melt-out of ice blocks (e.g. Cheel and Rust, 1986), (7) tsunamis (e.g. Matsumoto et al., 2009), (8) rapid sedimentation (e.g. Lowe and LoPiccolo, 1974; Lowe, 1975; Postma, 1983) and overloading (e.g. Moretti et al., 2001; Moretti and Sabato, 2007; Owen and Moretti, 2008), (9) movement of near-surface, gravity slides (e.g. Owen and Moretti, 2008), (10) asteroid impacts (e.g. Simms, 2007), (11) channel erosion (Dasgupta, 1998) or, (12) earthquakes (e.g. Ambraseys and Sarma, 1969; Audemard and De Santis, 1991; Obermeier, 1996a,b; Pope et al., 1997; Alfaro et al., 1999; Moretti et al., 1999; Rossetti, 1999; Jones and Omoto, 2000; Moretti, 2000; Tuttle et al., 2002; Wheeler, 2002; Rossetti and Santos, 2003; Audemard et al., 2005; Neuwerth et al., 2006; Moretti and Sabato, 2007; Pandey et al., 2009; among many others).

The deformation mechanisms and driving forces can be assessed by direct observation, since they depend upon the characteristics of the SSD structures, the sediments involved, and the depositional setting. However, different triggering agents can lead to the same SSD structures, so that no universal methodology exists for their identification. Many triggers would be considered as catastrophic events if they affect human society (e.g. floods, storms, earthquakes, tsunamis, and meteoritic impact). Consequently, the evaluation of the triggering mechanisms for SSD in sediments of Holocene age represents a potential tool for the assessment of geologic hazards.

In the scope of the tectono-sedimentary study of the middle to late Holocene sediments of the Santa Fe–Sopetrán (SFS) Basin (northern Colombian Andes), many SSD structures have been found. In total, eight localities within the middle Cauca Valley, middle to late Holocene fluvio-lacustrine terraces, show deformation affecting

* Corresponding author. Fax: +57 4 266 42 84.
E-mail addresses: fsuter@eafit.edu.co (F. Suter), jimartin@eafit.edu.co (J.I. Martínez), Maria.Velez.Caicedo@uregina.ca (M.I. Vélez).
[1] Fax: +57 4 266 42 84.
[2] Fax: +1 306 585 5433.

0037-0738/$ – see front matter © 2010 Elsevier B.V. All rights reserved.
doi:10.1016/j.sedgeo.2010.09.018

various types of soft deposits (Fig. 1). Historical earthquakes in the area, numerous recent debris-flow events and active landslides along the Cauca River Valley have been reported (e.g. Page and Mattson, 1981; Espinosa, 2009). The SFS Basin is a rapidly developing area, where the construction of a giant hydro-electric dam is in progress. It is located 30 km north of the city of Medellín, which has a population of 3 million.

In this study we focus on the recognition of mechanisms that triggered four deformed intervals in one middle to late Holocene sedimentary succession of the SFS Basin. This exercise is of unique value as it extends the geological hazard database for the middle Cauca Valley area down to the middle Holocene (about 7000 years BP). Data were collected by measurements and direct observation in the field. Paleocurrent measurements were taken on trough cross-beds in the sand layers.

1.1. Geological setting and location of the Santa Fe–Sopetrán (SFS) Basin

The SFS Basin is a 20 km long depression of the middle Cauca Valley. It is located between the Central and Western uplifting Cordilleras (e.g. Restrepo-Moreno et al., 2009), on the transcurrent Cauca–Romeral fault system (RFS, Fig. 1A and B), which outlines the suture between Cretaceous accreted oceanic basement to the west and Paleozoic to Cretaceous metamorphic and igneous basement to the east (e.g. Paris et al., 2000; Taboada et al., 2000; Fig. 1A and B). The RFS extends along the northern Andes from Guayaquil (Ecuador) to the Caribbean coastal plains of Colombia (Fig. 1A) and was responsible for two destructive earthquakes in the past 30 years: the 6.2 Mw in 1999 in the city of Armenia (Ingeominas, 1999) and the 5.5 Mw one in 1983 in the city of Popayán (Lomnitz and Hashizume, 1985). In the SFS Basin several neotectonic and paleoseismological studies have

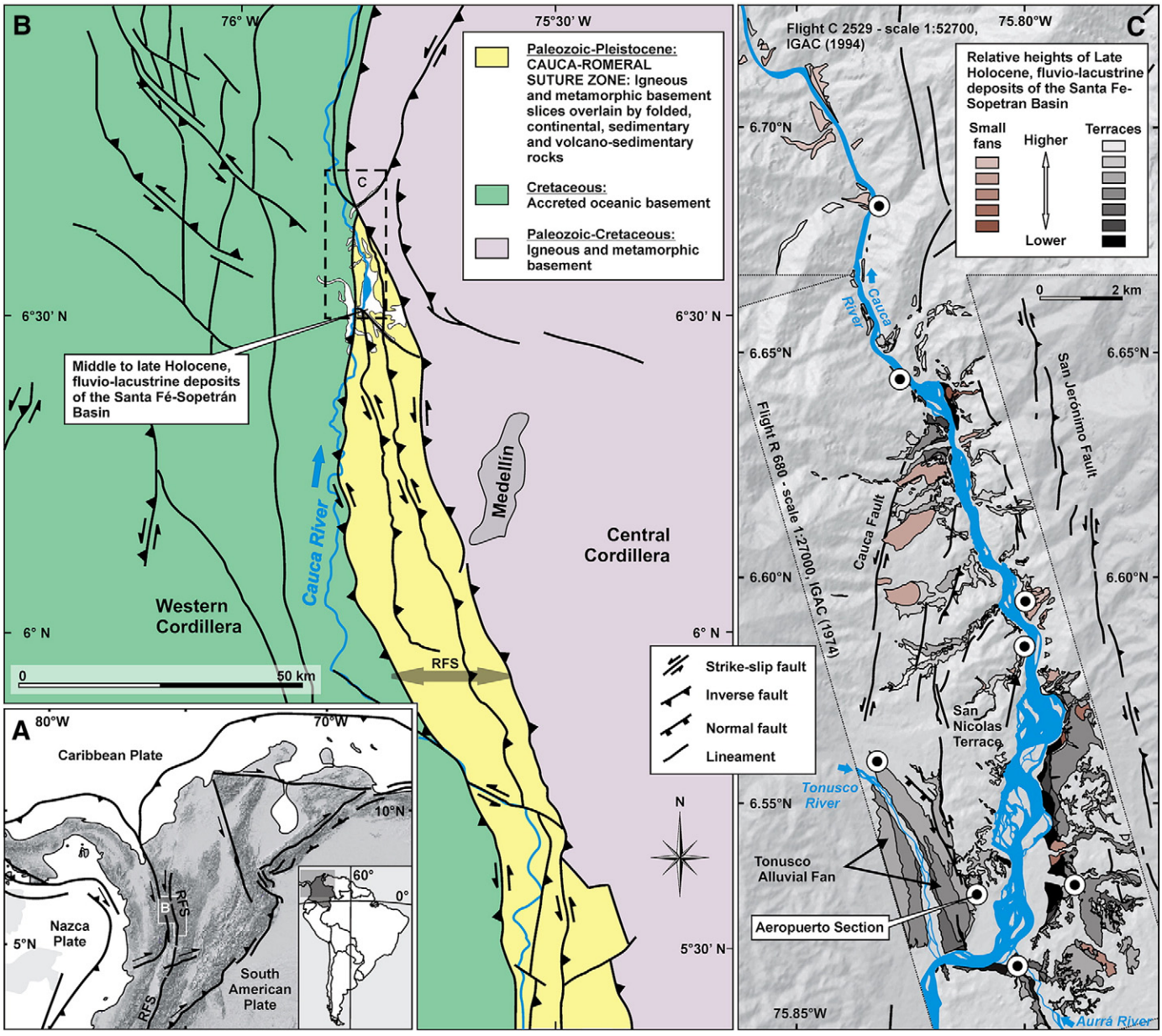

Fig. 1. (A) Neotectonic framework of the Colombian Andes, modified from Suter (2008). (B) Simplified geologic map of the middle Cauca Valley. Note the location of Medellín and the middle to late Holocene fluvio-lacustrine deposits (in white) of the Santa Fe–Sopetrán (SFS) Basin (modified from Mejía et al., 1983; Gómez et al., 2007). RFS: Cauca–Romeral Fault System. (C) Geomorphological map of the northern part of the SFS Basin, showing the relative heights of terraces and fans. Frames and numbers of aerial photograph flights used for mapping are indicated. Faults located out of frames were mapped on flight M-1422 (Instituto Geográfico Agustin Codazzi, Bogotá) and on 30 m resolution radar based DEM (USGS). Dots indicate localities where soft-sediment deformation structures were found, among them the Aeropuerto section.

been carried out on particular faults (Arias, 1981; Mesa and Lalinde, 2001; Morales, 2003; Lalinde et al., 2009), as well as one broad neotectonic study of the area (Campo and Mejía, 1981). However, the paucity of the often controversial data dealing with recent fault activity prevents the development of a precise model to explain the presence of the SFS inter-Andean Basin at 500 m elevation in an uplifting mountain chain. The SFS Basin genesis is closely related to the Late Cenozoic kinematics of the transcurrent RFS and possibly to other, cross-cutting fault systems (Suter et al., 2008b). The depression is classified as a pull-apart basin (Suter and Martínez, 2009).

1.2. Holocene fluvio-lacustrine deposits of the Santa Fe–Sopetrán Basin

Inter-Andean, folded, continental sedimentary rocks of the Eocene–Oligocene Amagá, and the late Miocene volcano-sedimentary Combia Formations (e.g. Grosse, 1926; Mejía et al., 1983; Parra, 1997; Ramírez et al., 2006) lie on the SFS Basin floor. They are overlain by coarse alluvial fan deposits of the Late Miocene–Pliocene El Tunal and El Goyas, and the Pleistocene El Llano successions (Parra, 1997). Middle to late Holocene fluvio-lacustrine terraces represent the last depositional stage in the Basin (Page and Mattson, 1981; Ruíz et al., 2005). According to Page and Mattson (1981), at least three lacustrine terrace levels were deposited successively, in response to the damming of the Cauca River Valley as a consequence of mega-landslides. They also provided preliminary ^{14}C ages (cal. years BP) for these terrace sets, i.e. 3100, 1500, and 800 years BP. However, geomorphologic mapping and field surveys of the SFS Basin indicate the presence of a higher number of terraces (Fig. 1C) and also show that the terrace deposits are not only lacustrine in origin, but also fluvial (Suter and Martínez, 2009; García et al., accepted for publication). South of the Basin, sedimentary sections show high-energy deposits that have been interpreted as braided river deposits on low-inclined alluvial fans. These sedimentary facies progressively evolve northwards to low-energy deposits interpreted as shallow lacustrine (Mesa, 2003; Ruíz et al., 2005) and floodplain environments. A palynofacies analysis and 11 AMS ^{14}C datings of the finely laminated San Nicolas terrace shows that the sedimentary succession was deposited from 6018 ± 106 to 1863 ± 297 cal. years BP (García et al., accepted for publication). Downstream, out of the basin limits, tectonics shows active uplift and the few remnants of sedimentary terraces show coarse debris-flow deposits originating on the valley slopes, which may have dammed the river course temporarily and generated swamp deposits upstream. The Aeropuerto section presented here is located south of the basin, in the south eastern edge and distal part of the low-inclined (slightly $<1°$ dip), Tonusco alluvial fan, where the Tonusco and Cauca rivers meet (Fig. 1C).

2. Results

2.1. Sedimentology and depositional environment

The Aeropuerto section (Fig. 1C) consists of a 25 m-thick succession of gravel, sand, silt and clay (Fig. 2). The gravel units are well sorted and clast-supported with rounded, imbricated pebbles. Some of the sand intervals show trough cross-bedding. Beds of fine sand, silts and clays are interbedded. Paleocurrent directions measured between deformed intervals 2 and 3 (Fig. 2) rotate clockwise from NW to SE, suggesting a rough NE direction. Lithofacies of the Aeropuerto section analysed herein are interpreted under the context of a modern alluvial fan (El Tonusco, Fig. 1C).

The bottom of this section is composed of 3 m of a thinning upward sequence, from clast-supported gravel to coarse-medium sand, with interbedded, thin, clayey lenses and isolated soft pebbles. Although cross-bedding is not observed, this interval is interpreted as a lateral migrating fluvial channel following Miall's (1990) classification criteria.

Overlying this basal unit, there is a 5 m-thick unit composed of two layers of fining upward sands to silt, intercalated with sand, silt and clay layers. The lowest one shows channels cutting through the underlying thin clay layer. In some silt layers, horizontal, flat pebbles lie parallel to the stratification. The entire unit is topped by a clay layer. This unit is interpreted to represent small-scale fluvial bars. In this unit the three lowermost deformed intervals, 1 through 3, were observed (Fig. 2).

This unit in turn is overlain conformably by a 2 m sand to gravel coarsening-upward sequence, which is overlain by a 3 m-thick gravel bed showing clayey and sandy lenses towards its top. According to Miall (1990), coarsening-upward sequences can be produced by prograding alluvial fans or deposited on steep slopes when there is abundant sediment supply. They can also be the product of an increase in the strength of a flow (Nichols, 1999). We interpret this unit as the product of a flow whose energy intensified to the point of being capable of transporting gravel clasts, followed by a channel fluvial bar.

On top of the gravel bed, there is a sand layer followed by a succession composed of a coarsening-upward silt to gravel sequence where trough cross-bedding is conspicuous. Capping, there is a 3 m silt unit with interbedded sand and clay layers. This part of the section is interpreted as a fluvial bar followed by flooding events. The uppermost deformed interval occurs at the base of this unit, i.e. 4 (Fig. 2).

The topmost unit is a 2 m clast-supported conglomerate which we interpret, despite the difficulty of reaching it, as a high-energy fluvial bar.

2.2. Soft-sediment deformation (SSD) structures and driving forces

The first and lowest deformed interval (1 in Fig. 2) is less than 1 m thick and occurs within a laminated alternation of clays and silts limited by medium sand at its base and coarse sand at its top (Fig. 3A). A 25–30 cm wide, pendulous load cast affects a channel of coarse sand at the top of the deformed interval (Fig. 3A). In the laminated alternation of clays and silts lying below, SSD structures include simple to pendulous load casts associated or not with flame structures (Fig. 3A, B, and C), and convolute to contorted laminations (Fig. 3C), similar in shape to roll-up structures (sensu Potter and Pettijohn, 1977). Lamination in the sinking sediment of the load casts is sometimes preserved but concave-upward following the shape of the load cast base (Fig. 3A). In some places, flame structures exhibit sharp fractures filled with the surrounding silt associated with angular pieces of clay floating in the silty matrix (Fig. 3B).

In this deformed interval the primary driving force was a gravitationally unstable density gradient which allowed denser sediment to sink into less dense sediment when it liquidized, and led to the load cast genesis (Fig. 3A and B). As the load cast developed, the underlying, finer sediment compensated its loss of volume with upward intrusions. Flame structures formed where this displacement of lighter sediment occurred vertically. At the base of the source layer, this motion occurred horizontally, which generated horizontal shear stress in the over-pressured, white clay layer, and allowed the silty laminae rolling up within the white clay to form contorted bedding (Fig. 3C). Minutes to hours after the trigger acted, pore-fluid pressure decreased, and grains settled and reorganized in a more compact arrangement (e.g. Moretti et al., 1999). Excess water should flow

Fig. 2. Sedimentary log of the Aeropuerto section. Large numbers refer to soft-sediment deformation (SSD) intervals. Rose diagram shows paleocurrent directions measured from trough cross-bedded sands. The large black arrow indicates the fining-upwards layer in which measurements were taken.

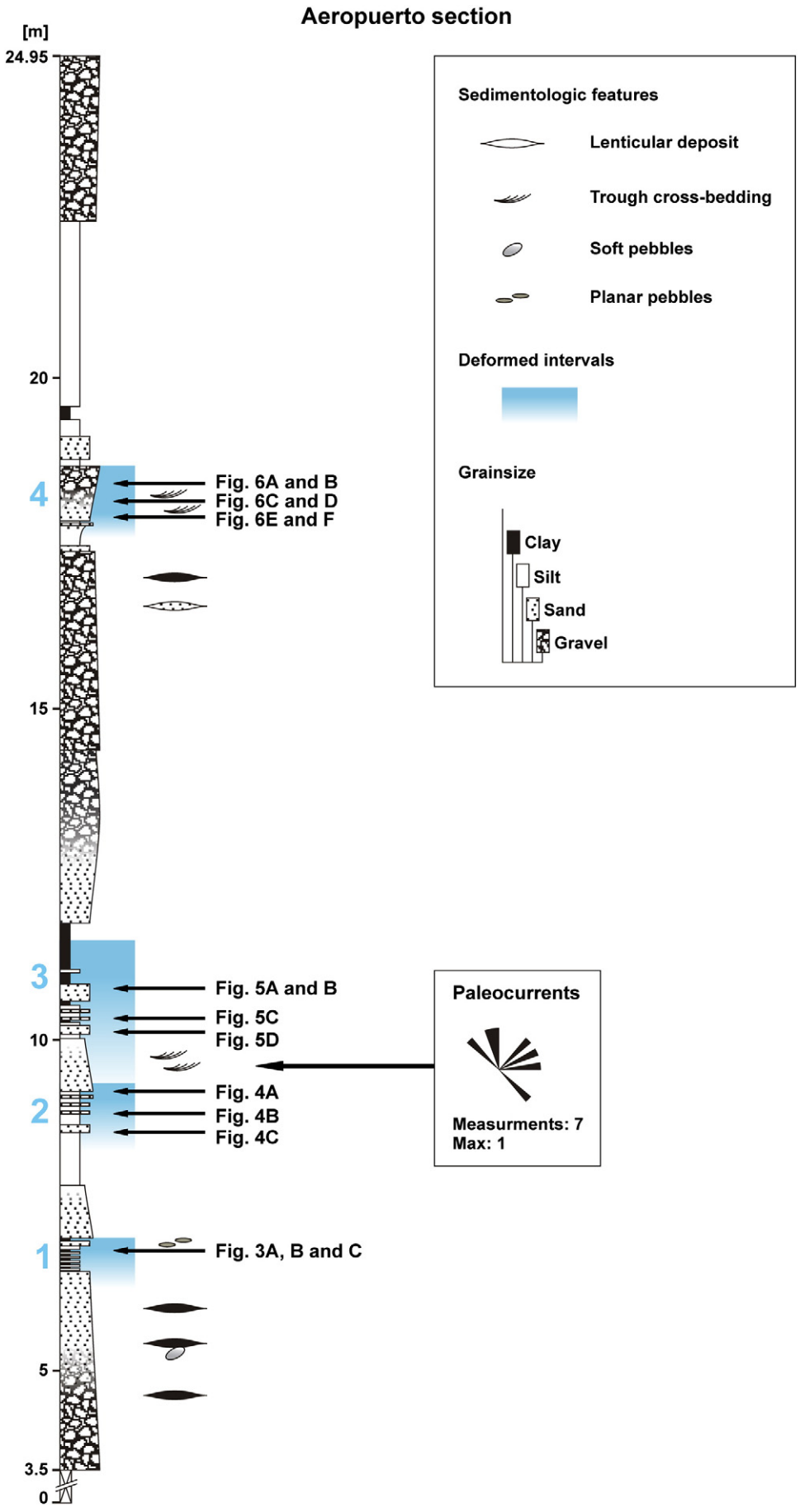
Aeropuerto section
[m]
24.95
20
15
10
5
3.5
0
4
3
2
1
Fig. 6A and B
Fig. 6C and D
Fig. 6E and F
Fig. 5A and B
Fig. 5C
Fig. 5D
Fig. 4A
Fig. 4B
Fig. 4C
Fig. 3A, B and C
Sedimentologic features
Lenticular deposit
Trough cross-bedding
Soft pebbles
Planar pebbles
Deformed intervals
Grainsize
Clay
Silt
Sand
Gravel
Paleocurrents
Measurments: 7
Max: 1

Fig. 3. The lowest deformed interval of the Aeropuerto section (1 in Fig. 2). (A) Large, white arrows point to load casts. Load cast on the right shows preserved, but bent laminations in the silt; small, white arrows point to the load-cast-associated flame structures. (B) Detail of A showing angular, broken pieces of white clay (small black arrows), and a fracture filled with silt, cutting the clay (small black arrow at the right), and small load casts (large white arrows) with an associated flame structure (small white arrow). (C) Detail of the white clay, located further right in the outcrop, showing contorted, silty beds (large, black arrows), and a small flame structure (small, white arrow). Vertical black bar represents the same thickness in A and C, i.e. ~10 cm.

upwards through the sedimentary pile. However, when porosity barriers exist, water cannot escape upwards as a fluid drag seeping through the porosity barrier. Rather, it bursts out through the top layer (Nichols et al., 1994). We interpret the fractures and angular broken pieces of white clay in the silt as driven by fluidization (vertical shear, sensu Owen, 1996).

The second deformed interval of this section (2 in Fig. 2) is 1 m thick. It occurs within an alternation of clayey silt with fine to medium sands, underlain by an 80 cm-thick layer of clayey silt, and overlain by a thinning upward, coarse sand layer. At the top of this interval, small, conjugate, normal faults cut the last clayey silt layer. The hanging wall block falls southwards, i.e. to the left of the outcrop (Fig. 4A). Below this faulted layer, the alternation of clayey silt with fine sands shows a rolled-up sand layer (Fig. 4B). At the base of this deformed interval, pendulous load casts of fine sand in clayey silt are associated with flame structures pointing southwards (Fig. 4C).

Load casts associated with flame structures show denser sediment which had sunk into less dense sediment. However, unidirectional flame structures in association with the overlying, rolled-up sand layers and the normal faults which testify to horizontal extension in the uppermost deformed layer (Fig. 4A), indicate that during liquefaction, a horizontal shear stress was acting in the sediment together with a gravitationally unstable density gradient.

The third deformed interval (3 in Fig. 2) occurs within a 1.5 m-thick alternation of fine sands, silts and clays (Figs. 2 and 5). The uppermost SSD structure is a dyke of medium sand, which contains pieces of the host silt to fine-sand layer. In the outcrop cross-section, it appears as a 6 to 10 cm wide, irregularly shaped patch of sand

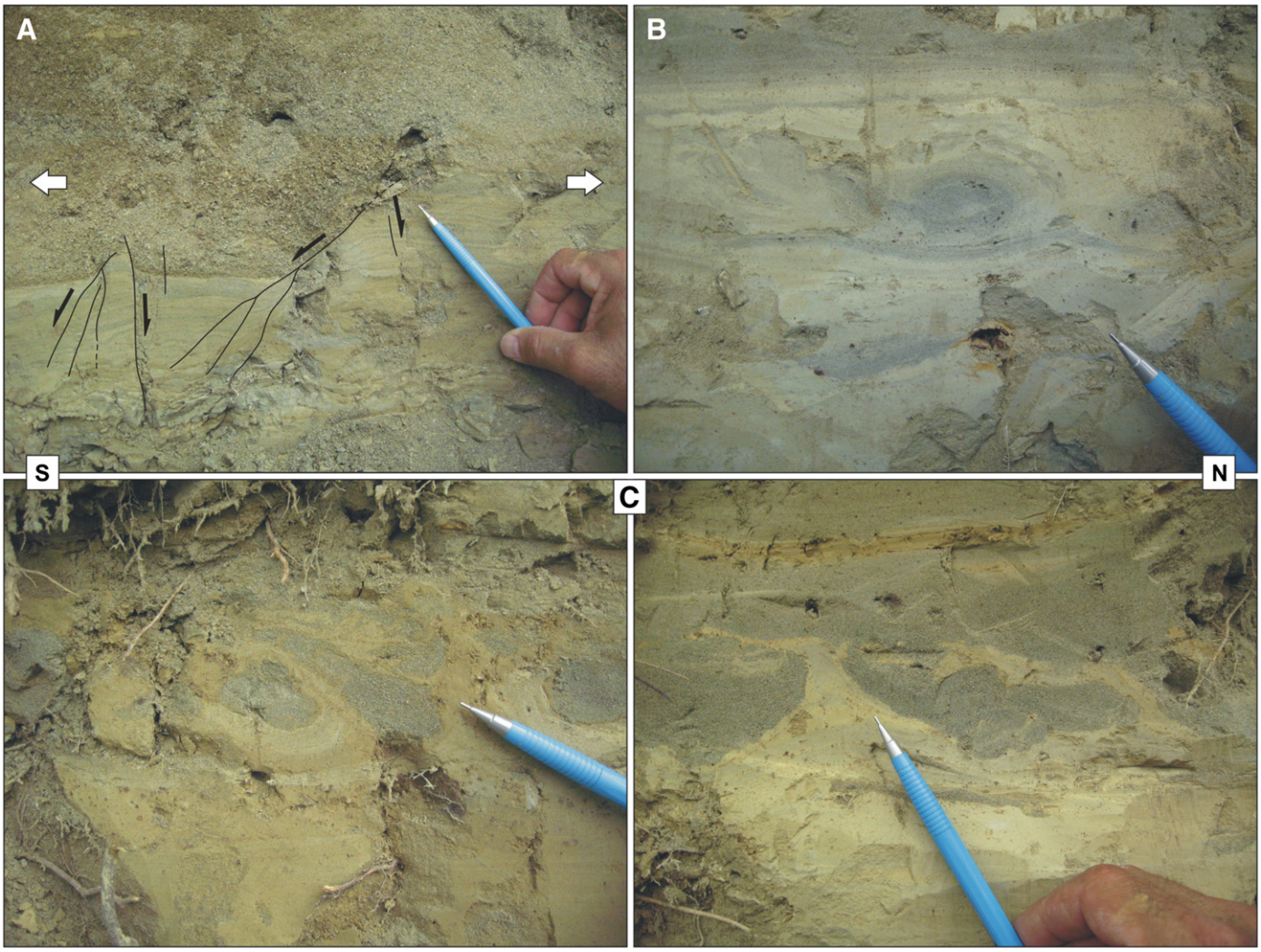

Fig. 4. Second deformed interval of the Aeropuerto section (2 in Fig. 2): (A) Uppermost deformed layer showing conjugate normal faults. The hanging wall block falls southwards. White arrows indicate the direction of extension. (B) A rolled-up fine-sand layer in the intermediate deformed layer. (C). The lowermost deformed layer shows pendulous load cast with associated south-pointing flame structures.

(Fig. 5A). The source layer is a normal graded sand layer located 1.5 m below. The sand intrusion completely crosses the deformed interval. The base of the fine silty sand host layer shows simple to pendulous load casts sinking in a silty clay layer, with associated flame structures. The latter sometimes point southwards (Fig. 5B). At the base, deformations encompass small size, south-pointing intrusions of clays into silt (Fig. 5C) or medium sand (Fig. 5D); millimetric, detached pseudonodules (Owen, 2003) of fine sand into silts; southward overturned pieces of a millimetre-thick, fine sand layer (Fig. 5C); and thrusted pieces of the latter layer.

As in the second deformed interval, the combination of load casts with southward oriented features such as flame structures, inclined, upward intrusions and overturned fragments, indicates a combination of driving forces acting together during liquefaction, i.e., a horizontal shear stress together with a gravitationally unstable density gradient (Fig. 7). In comparison with the second interval, here the horizontal shear stress seems to have been weaker because layer fragments are overturned and not rolled up. Not each flame structure is southward oriented such as in part 2, and extensional faults were not observed. The source layer of the clastic dyke (see Obermeier, 1996a,b) is sealed by an overlying, much less permeable, clayey layer (Fig. 5D) which acted as a porosity barrier during liquefaction. The pore-water overpressure could have been released by the sudden intrusion across the overlying layers by fluidization (vertical shear, sensu Owen, 1996).

The uppermost deformed level (4 in Figs. 2 and 6) is 1.3 m thick. It occurs within a coarsening-upward sand layer overlying a laterally continuous, 2–3 cm-thick silt layer. The contact between both layers shows millimetric to centimetric sized, irregularly shaped or bifurcate upward intrusions of silt in the sand (Fig. 6C, E and F). Immediately above the latter, the sand exhibits convolute laminations (e.g., Allen, 1977; Fig. 6C and D). The uppermost SSD structures are water-escape cusps (Fig. 6A), and dish and pillar structures (Lowe and LoPiccolo, 1974; Lowe, 1975; Fig. 6B).

The shape of the silt injections, in combination with the lateral continuity of the layer, which does not have considerable variations in thickness, leads to the interpretation of these deformation structures as driven by a gravitationally unstable density gradient. In the overlying sands, convolute laminations, water-escape cusps, and dish and pillar structures are associated. According to Lowe (1975): “there is a general consensus that convolute lamination is a complex form of load structure”. Owen (1996) attributes some convolute laminations to a reversed bulk-density gradient on sand-on-sand contacts. However, such as herein, convolute laminations are in many cases associated with water-escape structures (e.g. Lowe and LoPiccolo, 1974; Lowe, 1975; Mills, 1983; Cheel and Rust, 1986;

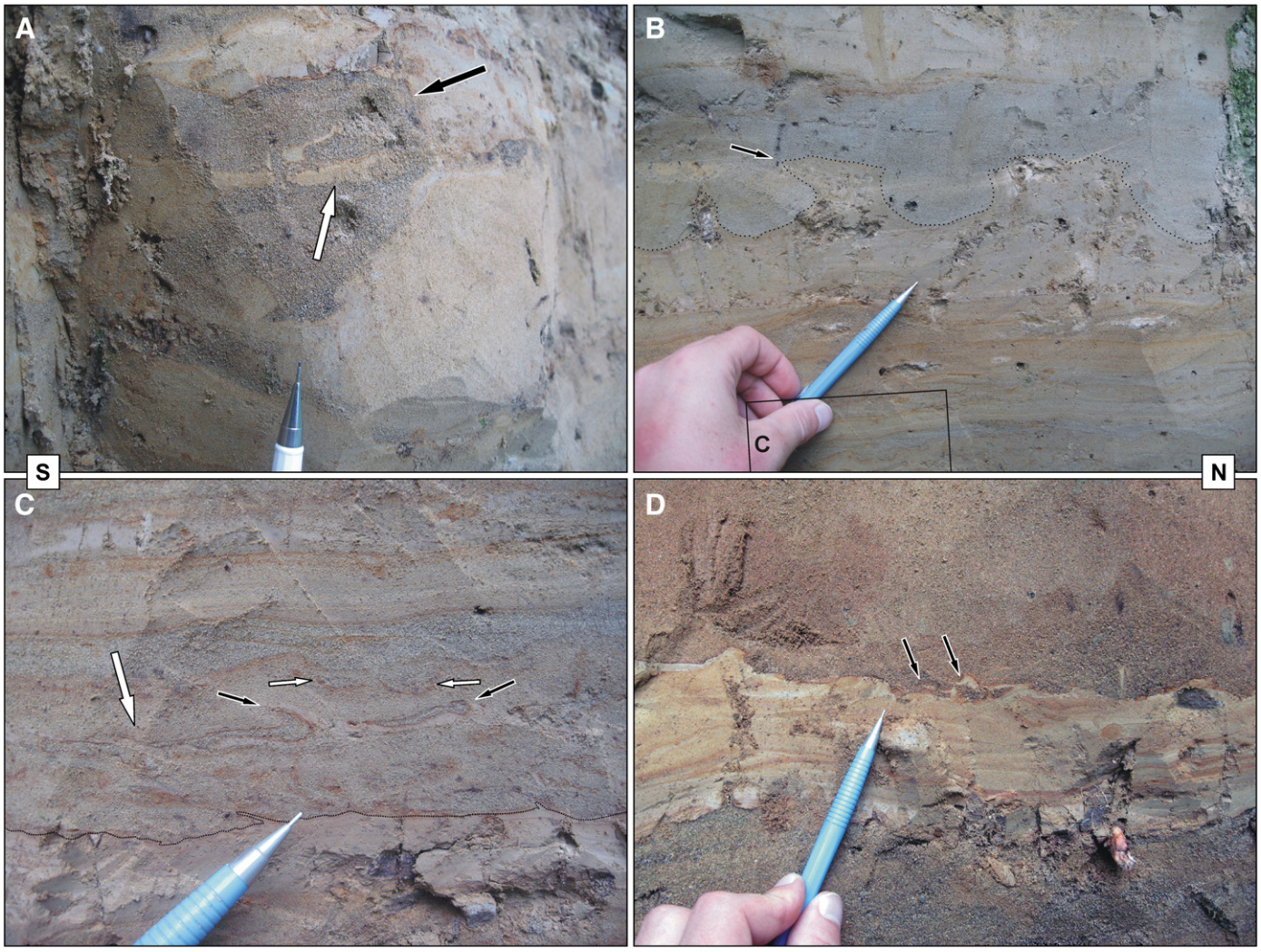

Fig. 5. Third deformed interval of the Aeropuerto section (3 in Fig. 2). (A) Clastic dyke of medium sand intruding a silt to fine-sand layer (black arrow). The white arrow points to a silty plug of the host sediment. (B) Load casts of silt into clays. Dotted line underlines the layer limit. The black arrow indicates an associated leftwards flame structure. (C) Detail of B. Thin alternation of fine sand, silt and clay, overlying a thick clay layer. Flame structures at the top of the basal clay layer point southwards, whereas a thin, broken fine-sand layer displays its broken overturned piece ends (black arrows). A piece of this sand layer overthrusts another broken piece of the same layer southwards (large white arrow). Small, white arrows point to detached pseudonodules of the overlying fine-sand layer. (D) Lowermost deformed layer of this interval showing flame structures pointing southward (black arrows). Sand at the base may be the source layer of the clastic dyke shown in A.

Owen, 1996; Rossetti, 1999). Thus, in this deformed interval, a combination of bulk-density heterogeneities (localised gravitationally unstable density gradients) and fluidization (vertical shear, sensu Owen, 1996) may have driven the deformation.

3. Discussion

3.1. Triggers of SSD in the Aeropuerto section

Owing to the fluvial depositional environment of the Aeropuerto outcrop presented here, possible triggering mechanisms for these SSD are: (1) channel erosion, (2) near-surface gravity slides, (3) cyclical pressure fluctuations associated with turbulent flow, (4) impulsive stress associated with flow fronts, (5) rapid artesian water rise, (6) rapid sedimentation and overloading, (7) asteroid impacts, and (8) earthquakes.

In the Aeropuerto section, concave-upward, inclined, channel erosional morphologies similar to the one described by Dasgupta (1998) do not occur. Additionally, evidence of gravitational slides is absent. Furthermore, none of the deposits testify to some turbulent flow. Consequently, channel erosion, gravity slides and cyclical pressure fluctuations or impulsive stresses associated with turbulent flows, respectively, can be discarded as potential triggers.

In the lowermost deformed interval (1 in Fig. 2), fractures which cross-cut the white clays might have been triggered by rapid artesian water rise. However, these fractures cut sharply across flame structures, which were previously deformed. There, vertical water movements occurred but they did not trigger liquefaction. In the second and third deformed intervals (2 and 3 in Fig. 2), this triggering agent is inconsistent with the horizontal shear stress needed to form asymmetric deformed structures. In the uppermost deformed interval (4 in Fig. 2), deformation structures generated by fluidization suggest an upward water seepage, rather than a rapid ascent through the sediment. Furthermore, structures typical of rapid pore-water movements were not observed (Li et al., 1996; Massari et al., 2001).

Deformed intervals 1, 2, and 3 do not show any evidence of rapid sedimentation, since sediments are dominated by clast-supported gravels interbedded with low to medium energy deposits (Fig. 2). The association of convolute lamination with water-escape cusps and dish structures, observed in the topmost deformed interval (4 in Fig. 2 and

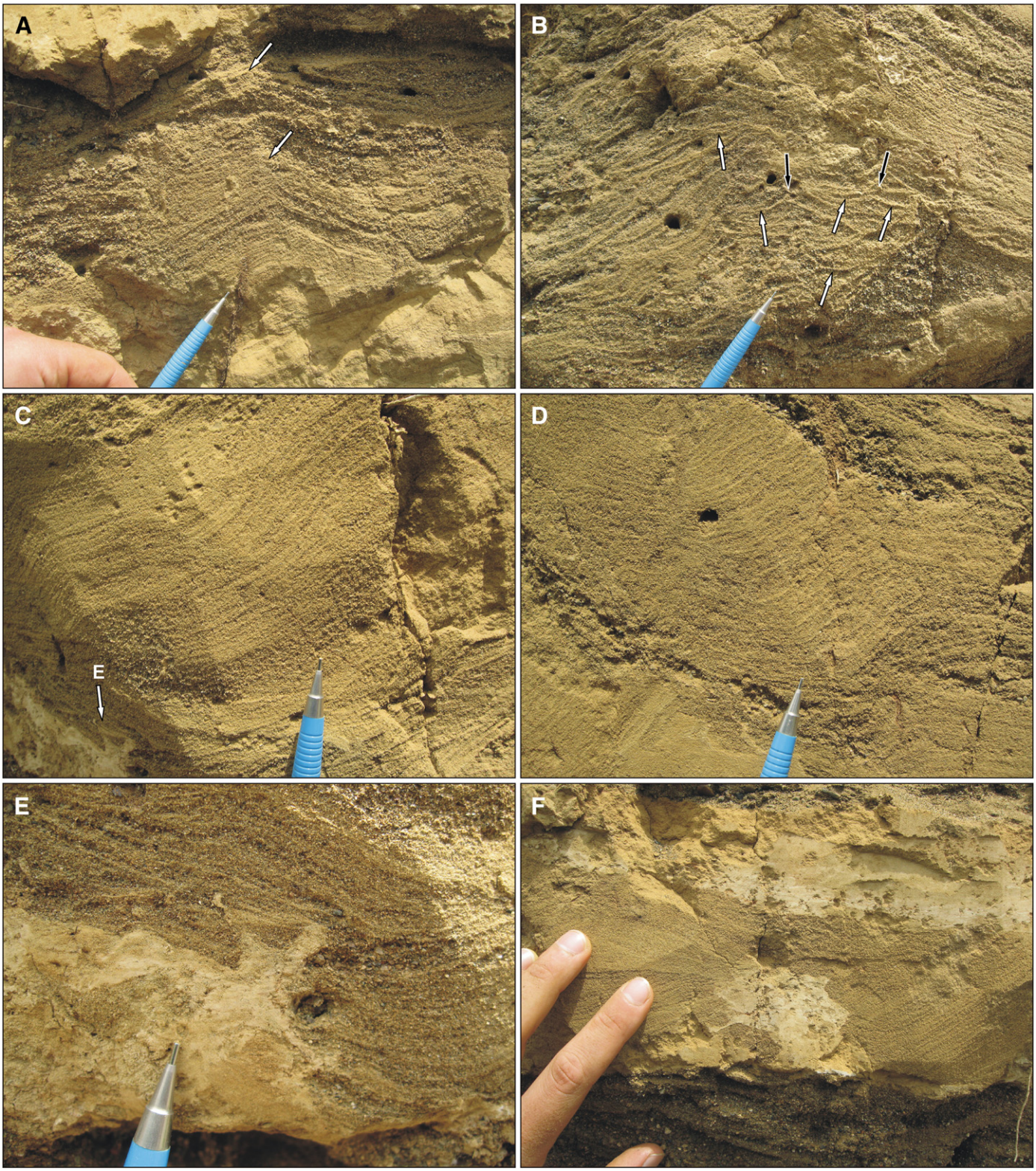

Fig. 6. Uppermost deformed interval of the Aeropuerto section (4 in Fig. 2). Grain size of affected sediment ranges from medium to coarse sand, including a thin silt layer at the base. (A) Water-escape cusps (white arrows). (B) Concave-upward dish structures (white arrows) and pillars (black arrows). (C) and (D) Convolute lamination. (E) and (F) Irregularly shaped injections of white silt into medium sand.

6A, B, C and D), however, is characteristic of unstable and rapidly deposited sediments (Lowe and LoPiccolo, 1974; Lowe, 1975; see also Owen, 1996). Since overloading is a trigger which acts during sedimentation and needs rapid deposition of denser sediment over a water-saturated, less dense substrate (e.g. Moretti et al., 2001; Owen and Moretti, 2008), the upwards, irregularly shaped injections of the underlying white silt into the medium sand may have been triggered by overloading (Fig. 6E and F). Deformation structures in the fourth

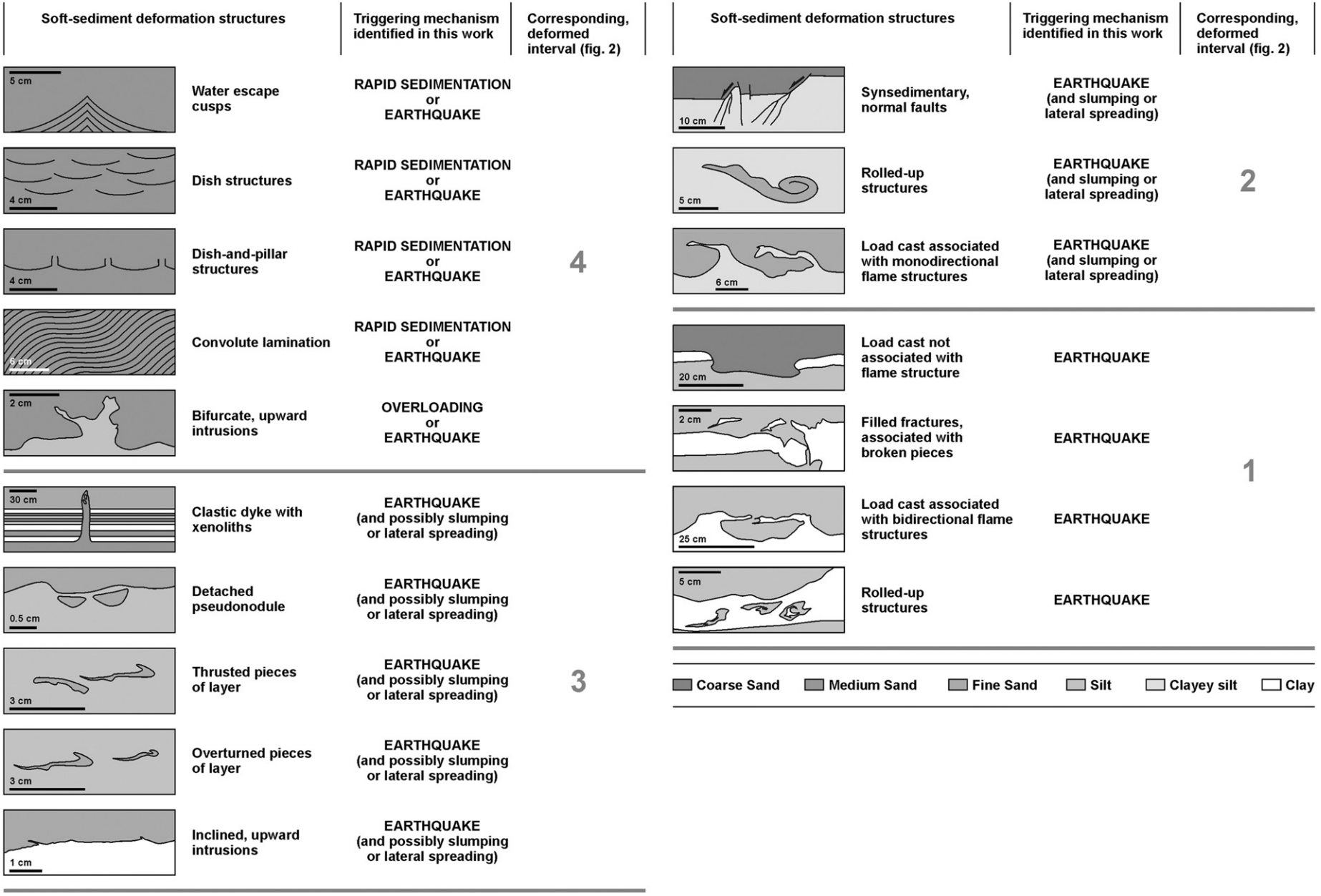

Fig. 7. Summary of the 17 types of soft-sediment deformation structures found in each of the 4 deformed intervals of the Aeropuerto section, with their respective triggering mechanism identified in the scope of this study. Numbers correspond to the deformed interval they belong to, labelled in Fig. 2. Soft-sediment deformation structures appear in stratigraphic order, except for deformed interval no. 3, where the clastic dyke crosscuts the entire deformed interval.

interval, thus, may have been triggered by rapid sedimentation and overloading, although earthquakes or other disturbances cannot be excluded (Lowe, 1975; Fig. 7).

The alternation of deformed and undeformed intervals in the Aeropuerto section makes the hypothesis of asteroid impact highly unlikely, considering that there are four deformed intervals together. Such an impact, if it occurred, might have triggered one event among these four. Nevertheless, an extraordinary areal extent of SSD (see Simms, 2007) cannot be proved, because only two other older SSD sites in Colombia have been reported, i.e. in the Plio-Pleistocene, Zarzal and Mesa Formations (Neuwerth et al., 2006; Suter et al., 2008a; Carlos Guzman, pers. comm.). Furthermore, no mention of a possible meteoritic impact exists in the late Holocene finely laminated records of northern South America (e.g. Rodbell et al., 1999; Peterson et al., 2000; Moy et al., 2002; Riedinger et al., 2002; Peterson and Haug, 2006).

Conversely, episodic triggers whose recurrence time is long enough to allow sufficient sediment accumulation in between the events, would match with this alternation. For SSD structures of the Aeropuerto section deposits, a seismic trigger appears to be the most likely, although deformation structures in the uppermost interval are likely to have been triggered by rapid sedimentation and overloading (Fig. 7).

The slope gradient of the low-inclined Tonusco alluvial fan (slightly $<1°$ dip) is too low to create shear parallel to the sediment surface observed in deformed intervals 2 and 3 (see Moretti et al., 2001). Paleocurrent directions measured on top of the second deformed interval are inconsistent with the direction indicated by the unidirectional flame structures lying below. In this deformed interval, the 1 m-thick vertical superposition of (from base to top) southward pointing flame structures, rolled-up structures and conjugate, normal, synsedimentary faults (Fig. 7), in combination with a seismic trigger, suggests that slumping or lateral spreading of the overlying sedimentary package may have occurred after fracturing when the underlying layers liquefied during an earthquake (e.g., Hansen et al., 1965; Obermeier, 1996a,b; Audemard et al., 2005; Suter et al., 2008b). Slumping or lateral spreading are probably the trigger of the horizontal shear in the second deformed interval and possibly also in the third deformed interval, although horizontal shear stress seems to have been less intense and synsedimentary faults were not observed (Fig. 7).

3.2. Evaluation of earthquake magnitude and recurrence time in the Santa Fe–Sopetrán Basin

Considering the Aeropuerto section together with the eight Late-Holocene, fluvio-lacustrine sediment localities presenting SSD structures in the SFS Basin (that extend over 20 km; Fig. 1C), a seismic trigger would be supported by the areal extent of deformed intervals following Wheeler's (2002) tests 2 and 3 and Obermeier's (1996a) criterion 4. This hypothesis is in agreement with the neotectonic activity of the Romeral Fault System (Campo and Mejía, 1981; Morales, 2003) and the available paleoseismological data (Arias, 1981; Mesa and Lalinde, 2001; Lalinde et al., 2009).

To be registered in the sedimentary record, the magnitude of an earthquake should be at least 4.5 Mw (e.g., Marco and Agnon, 1995). Scott and Price (1988) suggest that a magnitude of 7 does not significantly affect sediments beyond 20 km. Considering that 20 km is the maximum distance between sites where SSD structures have been observed in the SFS Basin, and assuming that they occurred simultaneously, earthquakes of a magnitude between 6 and 7 with the epicentre located somewhere in the Basin would have been required (refer also to Castilla and Audemard (2007) and references therein for liquefaction distribution versus earthquake magnitudes).

Assuming that the ages of the Aeropuerto Section alluvial fan deposits range between 7000 and 1500 years BP (Page and Mattson, 1981; García et al., accepted for publication) and considering that only three deformed intervals were triggered by earthquakes, a maximum mean recurrence time for 6 to 7 Mw earthquakes in the SFS Basin should be in the order of less than 1850 years. More dates are on the way and will provide a more precise chronology for the earthquake frequency in the SFS Basin.

4. Concluding remarks

1. Results of this study show that an accurate evaluation of SSD triggering mechanisms needs several conditions: (1) the understanding of the environmental conditions at the time of sediment deposition and shortly after, and (2) a detailed analysis of the driving force systems. In the particular case discussed here, most possible triggers can be discarded by combining (1) and (2). Nevertheless, for one interval, one or more triggers remained possible.
2. Deformation structures in both intermediate deformed intervals of the Aeropuerto section were probably triggered by seismic waves, and are linked to slumping or lateral spreading processes. Deformation in the lowermost interval was also possibly triggered by an earthquake, but without evidence of slumping or lateral spreading. The uppermost deformed interval was likely triggered by overloading and rapid sedimentation, although a seismic trigger cannot be discarded.
3. Regarding the seismic trigger, both the 20 km lateral extent and the vertical recurrence of the deformation intervals reinforce our interpretation. However, precise time correlations will test our hypothesis.
4. Mw between 6 and 7 are necessary to affect soft sediments along the 20 km long SFS Basin. As the sediments affected are middle to late Holocene in age, and record at least 3 earthquakes, decision-makers should seriously consider the seismic risk involved in the development of infrastructure projects in the middle Cauca Valley and in the city of Medellín.

Acknowledgements

This work is part of the research project: "Past climate variability in the Neotropics: evidence from lake Cauca, Colombia" funded by the Leverhulme Trust (Grant: ID20050769). We thank Huber Echeverry for support in the field, as well as Franck Audemard (FUNVISIS), an anonymous reviewer, and Geraint Owen for their constructive comments which helped to improve the manuscript.

References

Alfaro, P., Estévez, A., Moretti, M., Soria, J.M., 1999. Structures sédimentaires de déformation interprétées comme seismites dans le Quaternaire du bassin du Bas Segura (Cordillère bétique orientale). Comptes Rendus de l'Académie des Sciences Paris, Sciences de la Terre et des planètes 328, 17–22.

Alfaro, P., Delgado, J., Estévez, A., Molina, J.M., Moretti, M., Soria, J.M., 2002. Liquefaction and fluidization structures in Messinian storm deposits (Bajo Segura Basin, Betic Cordillera, southern Spain). International Journal of Earth Sciences (Geol. Rudnsch.) 91, 505–513.

Allen, J.R.L., 1977. The possible mechanics of convolute lamination in graded sand beds. Journal of the Geological Society of London 134, 19–31.

Ambraseys, N., Sarma, S., 1969. Liquefaction of soils induced by earthquakes. Bulletin. Seismological Society of America 59, 651–664.

Arias, L.A., 1981. Actividad Cuaternaria de la Falla Espíritu Santo. Revista CIAF 6 (1–3), 1–16.

Audemard, F.A., De Santis, F., 1991. Survey of liquefaction structures induced by recent moderate earthquakes. Bulletin of the International Association of Engineering Geology 4, 5–16.

Audemard, F.A., Gómez, J.C., Tavera, H.J., Nuris Orihuela, G., 2005. Soil liquefaction during the Arequipa Mw 8.4, June 23, 2001 earthquake, southern coastal Peru. Engineering Geology 78, 237–255.

Campo, J.A., Mejía, E.S., 1981. Estudio dinámico y mapeo litológico de la zona de Falla Cauca entre el Municipio de Santa Fe de Antioquia y la Quebrada Noque. Unpublished, BSc Thesis, Universidad Nacional de Colombia, sede Medellín, 131 pp.

Castilla, R.A., Audemard, F.A., 2007. Sand blows as a potential tool for magnitude estimation of pre-instrumental earthquakes. Journal of Seismology 11, 473–487.

Cheel, R.J., Rust, B.R., 1986. A sequence of soft-sediment deformation (dewatering) structures in Late Quaternary subaqueous outwash near Ottawa, Canada. Sedimentary Geology 47, 77–93.

Dalrymple, R.W., 1979. Wave-induced liquefaction: a modern example from the Bay of Fundy. Sedimentology 26, 835–844.

Dalrymple, R.W., 1980. Wave induced liquefaction: an addendum. Sedimentology 27, 461.

Dasgupta, P., 1998. Recumbent flame structures in the Lower Gondwana rocks of the Jharia Basin, India — a plausible origin. Sedimentary Geology 119, 253–261.
Denis, M., Buoncristiani, J.F., Guiraud, M., 2009. Fluid-pressure controlled soft-bed deformation sequence beneath the surging Breiðamerkurjökull (Iceland, Little Ice Age). Sedimentary Geology 221, 71–86.
Espinosa, A., 2009. Enciclopedia de Desastres Naturales Historicos de Colombia. Memorias. XII Congreso Colombiano de Geología, Paipa, Boyacá, 7 al 11 de Septiembre.
Eyles, N., Clark, B.M., 1986. Significance of hummocky and swaley cross-stratification in late Pleistocene lacustrine sediments of the Ontario basin, Canada. Geology 14, 679–682.
García, Y.C., Martínez, J.I., Vélez, M.I., Yokoyama, Y., Battarbee, R., Suter, F., accepted for publication. Palynofacies analysis of the late Holocene San Nicolas terrace of the Cauca paleolake, northern South America. Palaeogeography, Palaeoclimatology, Palaeoecology.
Gómez, J., Nivia, A., Montes, N.E., Jiménez, D.M., Sepúlveda, M.J., Gaona, T., Osorio, J.A., Diederix, H., Mora, M., Velásquez, M.E., 2007. Atlas Geológico de Colombia, Escala 1:500.000, Planchas 5-05 y 5-08. Ingeominas Bogotá.
Greb, S.F., Archer, A.W., 2007. Soft-sediment deformation produced by tides in a meizoseismic area, Turnagain Arm, Alaska. Geology 35, 435–438.
Grosse, E., 1926. Estudio Geológico del Terciario Carbonífero de Antioquia en la parte occidental de la Cordillera Central de Colombia: Berlín, Verlag Von Dietrich Reimer (Ernst Vohsen). 361 pp.
Hansen, W.R., Schmidt, R.A., Bedford, B., Calderwood, K.W., Ganopole, G., Hamilton, J.A., Helmuth, D.N., Moening, H.J., Richter, D.H., 1965. Effects of the earthquake of March 27, 1964, at Anchorage, Alaska. U. S. Geological Survey Professional Paper. U. S. Geological Survey, Reston, VA, United States, pp. A1–A68.
Ingeominas, 1999. Terremoto del Quindío (Enero 25 de 1999), informe técnicocientífico. INGEOMINAS, Bogotá, Colombia.
Jones, A.P., Omoto, K., 2000. Towards establishing criteria for identifying trigger mechanisms for soft-sediment deformation: a case study of Late Pleistocene lacustrine sands and clays, Onikobe and Nakayamadaira Basins, northeastern Japan. Sedimentology 47, 1211–1226.
Lalinde, C., González, A., Caballero, H., 2009. Evidencia paleosísmica en el segmento de falla Sopetrán o San Jerónimo Segmento 5. Boletín de Geología 31–2, 23–34.
Lee, J.R., Phillips, E.R., 2008. Progressive soft sediment deformation within a subglacial shear zone — a hybrid mosaic–pervasive deformation model for Middle Pleistocene glaciotectonised sediments from eastern England. Quaternary Science Reviews 27, 1350–1362.
Li, Y., Craven, J., Schweig, E.S., Obermeier, S.F., 1996. Sand boils induced by the 1993 Mississippi River flood: could they one day be misinterpreted as earthquake-induced liquefaction? Geology 24, 171–174.
Lomnitz, C., Hashizume, M., 1985. The Popayan, Colombia, earthquake of 31 March 1983. Bulletin. Seismological Society of America 75, 1315–1326.
Lowe, D.R., 1975. Water escape structures in coarse grained sediments. Sedimentology 22, 157–204.
Lowe, D.R., LoPiccolo, R.D., 1974. The characteristics and origins of dish and pillar structures. Journal of Sedimentary Petrology 44, 484–501.
Maltman, A., 1994. The Geological Deformation of Sediments. Chapman & Hall, London. 362 pp.
Marco, S., Agnon, A., 1995. Prehistoric earthquake deformations near Massada, Dead Sea graben. Geology 23, 695–698.
Massari, F., Ghibaudo, G., D'Alessandro, A., Davaud, E., 2001. Water-upwelling pipes and soft-sediment-deformation structures in Lower Pleistocene calcarenites (Salento, southern Italy). Geological Society of America Bulletin 113, 545–560.
Matsumoto, D., Naruse, H., Fujino, S., Jarupongsakul, T., Surphawajruksakul, A., Sakakura, N., 2009. Synsedimentary soft-sediment deformation in the 2004 Indian Ocean Tsunami deposit, Thailand. 27 th IAS Meeting of Sedimentology. Alghero, Italy, 20th–23th September, p. 268.
Mejía, M., Alvárez, E., González, H., Grosse, E., 1983. Plancha 130 — Santa Fe de Antioquia, Escala 1:100.000. Ingeominas, Bogotá.
Mesa, M.I., 2003. Propuesta de una metodología para identificar ritmitas, en un depósito lacustre del Río Cauca, Santa Fe de Antioquia, Antioquia, Colombia. Unpublished, MSc Thesis, Universidad Nacional de Colombia, sede Medellín, 85 pp.
Mesa, M.I., Lalinde, C., 2001. Actividad de la falla Espíritu Santo. Horizontes Naturales, Revista de la Facultad de Ciencias Exactas y Naturales de la Universidad de Caldas 4, 31–40.
Miall, A., 1990. Principles of Sedimentary Basin Analysis, 2nd ed. Springer-Verlag. 668 pp.
Mills, P.C., 1983. Genesis and diagnostic value of soft-sediment deformation structures — a review. Sedimentary Geology 35, 83–104.
Molina, J.M., Alfaro, P., Moretti, M., Soria, J.M., 1998. Soft-sediment deformation structures induced by cyclic stress of storm waves in tempestites (Miocene, Guadalquivir basin, Spain). Terra Nova 10, 145–150.
Morales, J.A., 2003. Evidecia neotectónica en la Falla Cauca Oeste, sector Puente de Occidente (Santa Fe de Antioquia). Unpublished, BSc Thesis, Universidad Nacional de Colombia, sede Medellín, 114 pp.
Moretti, M., 2000. Soft-sediment deformation structures interpreted as seismites in middle-late Pleistocene aeolian deposits (Apulian foreland, southern Italy). Sedimentary Geology 135, 167–179.
Moretti, M., Sabato, L., 2007. Recognition of trigger mechanisms for soft-sediment deformation in the Pleistocene lacustrine deposits of the Sant'Arcangelo Basin (Southern Italy): seismic shock vs. overloading. Sedimentary Geology 196, 31–45.
Moretti, M., Alfaro, P., Caselles, O., Canas, J.A., 1999. Modelling seismites with a digital shaking table. Tectonophysics 304, 369–383.
Moretti, M., Soria, J.M., Alfaro, P., Walsh, N., 2001. Asymmetrical soft-sediment deformation structures triggered by rapid sedimentation in turbiditic deposits (Late Miocene, Guadix Basin, Southern Spain). Facies 44, 283–294.
Moy, C.M., Seltzer, G.O., Rodbell, D.T., Anderson, D.M., 2002. Variability of El Niño/Southern Oscillation activity at millennial timescales during the Holocene epoch. Nature 420, 162–165.
Neuwerth, R., Suter, F., Guzman, C.A., Gorin, G.E., 2006. Soft-sediment deformation in a tectonically active area: the Plio-Pleistocene Zarzal Formation in the Cauca Valley (Western Colombia). Sedimentary Geology 186, 67–88.
Nichols, G., 1999. Sedimentology and Stratigraphy. Blackwell publishing. 355 pp.
Nichols, R.J., Sparks, R.S.J., Wilson, C.J.N., 1994. Experimental studies of the fluidization of layered sediments and the formation of fluid escape structures. Sedimentology 41, 233–253.
Obermeier, S.F., 1996a. Use of liquefaction-induced features for paleoseismic analysis — an overview of how seismic liquefaction features can be distinguished from other features and how their regional distribution and properties of source sediment can be used to infer the location and strength of Holocene paleo-earthquakes. Engineering Geology 44, 1–76.
Obermeier, S.F., 1996b. Using liquefaction-induced and other soft-sediment features for paleoseismic analysis. In: McCalpin (Ed.), Paleoseismology. : International Geophysics, 95. Academic Press, Elsevier, pp. 497–564.
Owen, G., 1987. Deformation processes in unconsolidated sands. In: Jones, M.E., Preston, R.M.F. (Eds.), Deformation of Sediments and Sedimentary Rocks: Geol. Soc. Spec. Publ., Geological Society of London, 29, pp. 11–24.
Owen, G., 1996. Experimental soft-sediment deformation structures formed by the liquefaction of unconsolidated sands and some ancient examples. Sedimentology 43, 279–293.
Owen, G., 2003. Load structures: gravity-driven sediment mobilization in the shallow subsurface. In: Van Rensebergen, P., Hillis, R.R., Maltman, A.J., Morley, C.K. (Eds.), Subsurface Sediment Mobilization: Geol. Soc. Spec. Publ., Geological Society of London, 216, pp. 21–34.
Owen, G., Moretti, M., 2008. Determining the origin of soft-sediment deformation structures: a case study from Upper Carboniferous delta deposits in south-west Wales, UK. Terra Nova 20, 237–245.
Page, W.D., Mattson, L., 1981. Landslide Lakes near Santa Fe de Antioquia. Revista CIAF 6 (1–3), 469–478.
Pandey, P., Kumar, R., Suresh, N., Sangode, S.J., Pandey, A.K., 2009. Soft-sediment deformation in contemporary reservoir sediment: a repository of recent major earthquake events in Garhwal Himalaya. Journal of Geology 117, 200–209.
Paris, G., Machette, M.N., Dart, R.L., Haller, K.M., 2000. Map and Database of Quaternary Faults and Folds in Colombia and its Offshore Regions. U. S. Geological Survey, Reston, VA, United States. 61 pp., 1 sheet.
Parra, L.N., 1997. El Terciario del Valle del Río Cauca al norte de la Barrera de Cangrejo - borde Oeste -. Unpublished, MSc Thesis, Universidad Nacional de Colombia, sede Medellín, 118 pp.
Peterson, L.C., Haug, G.H., 2006. Variability in the mean latitude of the Atlantic Intertropical Convergence Zone as recorded by riverine input of sediments to the Cariaco Basin (Venezuela). Palaeogeography, Palaeoclimatology, Palaeoecology 234, 97–113.
Peterson, L.C., Haug, G.H., Hughen, K.A., Röhl, U., 2000. Rapid changes in the hydrologic cycle of the tropical Atlantic during the last glacial. Science 290, 1947–1951.
Pope, M.C., Read, J.F., Bambach, R., Hofmann, H.J., 1997. Late Middle to Late Ordovician seismites of Kentucky, southwest Ohio and Virginia: sedimentary recorders of earthquakes in the Appalachian basin. Geological Society of America Bulletin 109, 489–503.
Postma, G., 1983. Water escape structures in the context of a depositional model of a mass flow dominated conglomeratic fan-delta (Abrioja Formation, Pliocene, Almeria Basin, SE Spain). Sedimentology 30, 91–103.
Potter, P.E., Pettijohn, F.J., 1977. Paleocurrents and Basin Analysis, 2nd ed. Springer-Verlag, New York. 296 pp.
Ramírez, D., López, A., Sierra, G., Toro, G., 2006. Edad y proveniencia de las rocas volcánico sedimentarias de la Formación Combia en el Suroccidente Antioqueño – Colombia. Boletín de Ciencias de la Tierra (ISSN: 0120-3630) 19, 9–26.
Restrepo-Moreno, S.A., Foster, D.A., Stockli, D.F., Parra-Sánchez, L.N., 2009. Long-term erosion and exhumation of the "Altiplano Antioqueño", Northern Andes (Colombia) from apatite (U–Th)/He thermochronology. Earth and Planetary Science Letters 278 (1–2), 1–12.
Riedinger, M., Steinitz-Kannan, M., Last, W.M., Brenner, M., 2002. A 6100 14 C record of El Niño activity from the Galápagos Islands. Journal of Paleolimnology 27, 1–7.
Rodbell, D.T., Seltzer, G.O., Anderson, D.M., Abbott, M.B., Enfield, D.B., Newman, J.H., 1999. An 15, 000-year record of El Niño-driven alluviation in Southwestern Ecuador. Science 283, 517–520.
Rossetti, D.F., 1999. Soft-sediment deformation structures in late Albian to Cenomanian deposits, Sao Luis Basin, northern Brazil: evidence for palaeoseismicity. Sedimentology 46, 1065–1081.
Rossetti, D.F., Santos Jr., A.E., 2003. Events of sediment deformation and mass failure in Upper Cretaceous estuarine deposits (Cametá' Basin, northern Brazil) as evidence for seismic activity. Sedimentary Geology 161, 107–130.
Ruíz, O.D., Sánchez, D.P., Parra, C.E., 2005. Un registro Holocénico de alta resolución: los lodos de La Batea. Santa Fe de Antioquia. Reporte y Perspectivas. Boletín de Ciencias de la Tierra 17, 109–116.
Scott, B., Price, S., 1988. Earthquake-induced structures in young sediments. Tectonophysics 147, 165–170.
Simms, M.J., 2007. Uniquely extensive soft-sediment deformation in the Rhaetian of the UK: evidence for earthquake or impact? Palaeogeography, Palaeoclimatology, Palaeoecology 244, 407–423.
Suter, F., 2008. Tectono-sedimentary study of the Interandean north Cauca Valley Basin, central western Colombia. Terre & Environnement 78 viii, 145 pp.

Suter, F., Martínez, J.I., 2009. Tectónica transpresiva Cuaternaria en la sutura de Romeral: ejemplo de la cuenca de Santa Fe–Sopetrán, Antioquia. Memorias, XII Congreso Colombiano de Geología, Paipa, Boyacá, 7 al 11 de Septiembre.

Suter, F., Neuwerth, R., Guzman, C., Gorin, G., 2008a. Depositional model of (Plio-) Pleistocene sediments in a tectonically active zone of Central Colombia. Geologica Acta 6 (3), 231–249.

Suter, F., Sartori, M., Neuwerth, R., Gorin, G., 2008b. Structural imprints at the front of the Chocó-Panamá indenter: field data from the North Cauca Valley Basin, Central Colombia. Tectonophysics 460 (1–4), 134–157.

Taboada, A., Rivera, L.A., Fuenzalida, A., Cisternas, A., Philip, H., Bijwaard, H., Olaya, J., Rivera, C., 2000. Geodynamics of the Northern Andes; subductions and intracontinental deformation (Colombia). Tectonics 19, 787–813.

Tuttle, M.P., Dyer-Williams, K., Barstow, N.L., 2002. Paleoliquefaction study of the Clarendon–Linden fault system, western New York State. Tectonophysics 353, 263–286.

Wheeler, R.L., 2002. Distinguishing seismic from nonseismic softsediment structures: criteria from seismic-hazard analysis. In: Ettensohn, F.R., Rast, N., Brett, C.E. (Eds.), Ancient Seismites, Boulder, Geological Society of America Special Paper, 359, pp. 1–11.